A Multivariable, Adaptive, Robust, Primary Control Enforcing Predetermined Dynamics of Interest in Islanded Microgrids Based on Grid-Forming Inverter-Based Resources

Amir Afshari, Masoud Davari, *Senior Member, IEEE*, Mehdi Karrari, *Senior Member, IEEE*, Weinan Gao, *Senior Member, IEEE*, and Frede Blaabjerg, *Fellow, IEEE*

***Abstract*— This paper proposes a multivariable, adaptive, robust (MAR) control strategy for islanded inverter-based resources (IBRs) operating as grid-forming inverters. The proposed method is employed in the inner control loop of the primary layer in the hierarchical or decentralized structures for the islanded operation of microgrids. The MAR control scheme is responsible for stabilizing IBRs' output voltage in autonomous operations of microgrids, considering mismatched input voltage disturbances from the grid side and a large amount of system uncertainty. The control methodology introduced in this paper does not rely on the system's physical parameters, such as microgrid topology, load dynamics, LCL filters, and output connectors. As a result, there is no need to know the nominal values or the bounds of uncertainties in system dynamics. The MAR control method uses online adaptation rules first to identify and then adjust the control parameters of the closed-loop system based on an arbitrary dynamic model. In other words, the MAR method replaces the actual dynamics of IBRs with predetermined dynamics of interest. Simulation results in the MATLAB/Simulink environment confirm the capability of the scheme introduced for the closed-loop stabilization and voltage regulation in the presence of disturbances and a significant amount of uncertainty under various case studies; moreover, comparative simulations by comparing the presented method with other studies using sliding mode control are provided. Finally, experiments verify the effectiveness and practicality of the proposed MAR control scheme.**

Manuscript received 11 August 2022; revised 20 January 2023; accepted 10 March 2023. This article was recommended for publication by Associate Editor M. Robba and Editor Q. Zhao upon evaluation of the reviewers' comments. The work of Masoud Davari was supported in part by the U.S.–Denmark Program funded by the Office of International Science and Engineering (OISE) through the U.S. National Science Foundation (NSF) through the NSF-OISE-IRES (International Research Experiences for Students) under Award 2152905, in part by the U.S. NSF Electrical, Communications and Cyber Systems-Energy, Power, Control, and Networks (ECCS-EPCN) under Award 1808279 and Award 1902787, in part by the dSPACE company, in part by the Verivolt company, in part by the Discovery and Innovation Award from the 2020–2021 University Awards of Excellence at Georgia Southern University, and in part by the Impact Area Accelerator Grant funded by Georgia Southern University—at which all experiments were conducted. *(Corresponding authors: Masoud Davari; Weinan Gao.)*

Amir Afshari is with the Department of Electrical and Computer Engineering, University of Wisconsin–Madison, Madison, WI 53706 USA (e-mail: afshari2@wisc.edu).

Masoud Davari is with the Department of Electrical and Computer Engineering, Georgia Southern University, Statesboro Campus, Statesboro, GA 30460 USA (e-mail: mdavari@georgiasouthern.edu; davari@ualberta.ca).

Mehdi Karrari is with the Department of Electrical Engineering, Amirkabir University of Technology (Tehran Polytechnic), Tehran 1591634311, Iran (e-mail: karrari@aut.ac.ir).

Weinan Gao is with the State Key Laboratory of Synthetical Automation for Process Industries, Northeastern University, Shenyang, Liaoning 110819, China (e-mail: gaown@mail.neu.edu.cn).

Frede Blaabjerg is with the AAU Energy, Aalborg University, 9220 Aalborg, Denmark (e-mail: fbl@energy.aau.dk).

Color versions of one or more figures in this article are available at https://doi.org/10.1109/TASE.2023.3262852.

Digital Object Identifier 10.1109/TASE.2023.3262852

***Note to Practitioners*—Inverter-based resources are integral parts of current and especially future power and energy systems; with increasing concerns about carbon footprints, the tendency to substitute traditional synchronous generators with inverter-based resources increases. This transition towards the widespread use of power electronics devices needs careful studies regarding the stability and control of power converters. Although existing studies are addressing potential control system challenges, they suffer from complex mathematical computations and the need for the system's preliminary information. With this in mind, this study proposes a multivariable, adaptive, robust control strategy for the inner voltage control loop of grid-forming inverters. This method utilizes online estimation algorithms to identify inverter-based resources' parameters and tune control system parameters simultaneously, making it applicable even to cases with slow parameter variations caused by aging or environmental changes. It can compensate for potential voltage disturbances from the grid side and enable the designer to replace undesirable dynamics of inverter-based resource units with arbitrary and stable dynamics of interest. In fact, unlike traditional methods that need control parameters and gains to be tuned to achieve a proper dynamic response, the control system designer can choose reference dynamics and enforce the closed-loop system to imitate the dynamical model selected. This model is usually chosen based on established priorities, such as response time and other transient behaviors. Moreover, this method does not require complex mathematical and algebraic calculations to design and implement. It can be easily applied to inverter-based resource units after selecting the desired reference dynamics, as shown through this study's experimental result. The above points give this method a competitive edge over the existing algorithms, especially in practical applications.**

***Index Terms*— Grid-forming inverter-based resources (GFM IBRs), multivariable, adaptive, robust (MAR) control, online adaptation rule, online estimation, predetermined dynamics of interest for islanded IBRs, primary control of islanded IBRs, voltage-sourced converters (VSCs).**

NOMENCLATURE

A. IBR's Variables

V_{odq}, I_{odq} IBR's output voltage and current in the dq frame.

I_{Ldq}	IBR's generated current in the dq frame.
V_{idq}	Terminal voltage (control input) in the dq frame.
V_{bdq}	Grid-side voltage (disturbance signal) in the dq frame.
$V_{\rm DC}$	DC-side voltage.
$I_{\rm DC}$, I_C	Controllable dc-source current and dc current delivered to IBRs.

B. IBR's Parameters

R_f, $R_{\rm DC}$	Output filter and dc-side resistances.
L_f	Output filter inductance.
C_f, $C_{\rm DC}$	Output filter and dc-side capacitances.
ω	Grid nominal frequency.
R_c	Output connector resistance.
L_c	Output connector inductance.

C. Control System Parameters

$G(s)$, $G_m(s)$	System and reference dynamics.
$\chi_m(s)$	Left interactor matrix associated with system dynamics.
K_H, $\Gamma(t)$	High frequency gain matrix and its estimate.
$r(t)$, $y_m(t)$	Reference input and output signals.
K_1^*, K_2^*, K_3^*	Nominal feedback gains.
η	System relative degree.
$g(t)$, $\tilde{\Psi}^*$, Ψ^*	Disturbance parametrization terms.
γ	Estimate of nominal control parameters.
Σ_1, Σ_2	Adaptation gains.
$e(t)$, $\delta(t)$	Estimation errors.
$\tau_{\rm DC}$	DC-side time constant.
K_P	DC-side proportional controller gain.

I. Introduction

RECENT advances in distributed energy resources, renewables, information theory, and communication technologies have led to significant utilization of microgrids [1], [2]—thereby integrating various inverter-based resources (IBRs) [3]. Traditionally, the hierarchical control structure has been applied to the control system design of microgrids, even modern ones. This structure consists of the primary, secondary, and tertiary control layers; see [4], [5], [6], [7], and [8]. Using this structure, and due to the flexibility and scalability of microgrids, they can operate in both grid-connected and islanded modes [9]. In the islanded operation, voltage and frequency stability is the primary objective of the microgrid control systems, which are realizable by employing GFM inverters and different types of GFM controllers operating in the primary control layer [10], [11], [12]. The primary layer is utilized to implement real-time voltage and frequency control algorithms [13]. Because of the volatile and uncertain nature of the renewables, disturbances, and systems' uncertainties, it is necessary to have a properly designed advanced control system for IBRs' operating as GFM units to have a smooth integration of IBRs into microgrids and a stable power supply for consumers.

In order to address these issues in the islanded mode or even grid-connected operations, various studies have been done in the literature [14]. For the case of grid-connected mode, a robust control algorithm is developed for unbalanced-grid conditions in [15]. A cascaded PI-based control strategy is employed to regulate the output voltage of voltage-sourced converters (VSCs) in [16]. A robust H_∞ controller is proposed in [17] to reject load currents as disturbances—it deploys the stationary reference frame to design the control algorithm. In [18], a cascaded structure including sliding mode and mixed H_2/H_∞ controllers is designed for the primary layer of ac microgrids, considering external load currents as disturbances. The methods presented in [19] and [20] solve the voltage stability problem of islanded microgrids using decentralized robust state and output feedback control algorithms, respectively. In [21], a decentralized sliding mode controller is designed for both grid-connected and islanded operation of microgrids considering nonlinear and unbalanced load conditions. The authors in [22] have proposed a robust decoupling pre-compensator for the autonomous operation of microgrids. This control structure only deals with norm bounded uncertainties and depends on the system's structure and topology. Voltage stabilization of islanded microgrids, considering plug-and-play functionality and robustness against microgrid topology changes, is addressed in [23]. A model predictive control algorithm for the voltage regulation of islanded ac microgrids is introduced in [24]. Considering uncertainties and load disturbances, a decentralized sliding mode controller for the islanded operation of microgrids is developed in [25]—it uses a second-order sliding mode control strategy based on a sub-optimal algorithm. It is noteworthy that the design of this control algorithm requires the structure and physical topology of the microgrid to be "*known*." The authors in [26] investigated the robust performance of a microgrid using a sliding mode control algorithm in both grid-connected and islanded operations.

In this regard, some studies use adaptive algorithms for controlling VSCs in microgrids. For example, an adaptive algorithm for the current controller of grid-connected VSCs is developed in [27]—it utilizes indirect adaptive algorithms based on identifying system parameters, which are needed to implement the proposed algorithm. Thus, the persistent excitation condition must be met, so convergence problems are inevitable in this method. The authors in [28] addressed voltage stability in islanded microgrids using an adaptive voltage controller. This control algorithm is solely responsible for a specific bound of systems uncertainty, so knowing the nominal values of system parameters is a must. Additionally, the existence of external disturbances is ignored in this method.

Most studies mentioned above have investigated the robust stability and control of microgrids under different conditions using robust control algorithms. But there are still some limitations in these algorithms that should be addressed. Control systems operate in various unknown operational environments with external disturbances and uncertainties. Additionally, component aging and even system failures can change system parameters. Thus, in practice, system parameters are expected

to change over time. In this regard, robust control algorithms are designed offline and have fixed parameters. They are usually based on prior knowledge of system parameters and designed for the worst case of uncertainties. This issue makes them often conservative; consequently, it can degrade the performance of the closed-loop system in instances—where uncertainties are not at their worst.

Additionally, it is always required to know the nominal values of parameters and bounds of their uncertainties in the design procedure of these algorithms. In addition to the constraints mentioned above, sliding mode controllers are usually suitable for rejecting matched uncertainties—thereby suffering from problems related to the reaching phase [29]. Therefore, according to the existing studies, the main drawbacks of the previously reported control algorithms are listed as: 1) they are unable to compensate for a large amount of uncertainty and mismatched disturbances; 2) system response may be too conservative for different operating conditions, especially in robust H_2/H_∞ algorithms; 3) due to the variation of system parameters over time, it is needed to constantly "*re-tune*" the controller's parameters to maintain the control system's performance.

In order to address the issues detailed above, this paper presents a multivariable, adaptive, robust control strategy based on an "*online*" estimation methodology—in direct contrast to what scholars have already investigated thus far—to guarantee the stability and robust performance of islanded ac microgrids. With the least prior information about the system and bounds of uncertainties, the proposed control algorithm performs online estimations, thereby identifying the uncertain system's parameters—which can change over time. It adjusts the control parameters to achieve the desired performance. The method presented utilizes a dynamic reference model or a predetermined dynamic model of interest (as an ideal and arbitrary stable dynamic system) expressing the expected and desired performance of the closed-loop system. It changes the behavior of the actual system in a way that its dynamic response matches the characteristics of the desired system selected using online adjustment rules; see Fig. 1 (left side) and [30], [31]. Therefore, there is a large degree of freedom to design and select the reference model. It should be pointed out that the control strategy introduced in this article is entirely different from the traditional adaptive droop studies. In existing research, either droop gains are adaptively changed using different measurements (e.g., see [32]) or the studies in which various adaptive algorithms are employed in the secondary layer of the hierarchical-based microgrids (e.g., see [33], [34], and [35]). Indeed, it may be utilized as the inner control loop of GFM inverters, whether in the hierarchical structure combined with other control layers or even in a decentralized structure with a decentralized energy management system.

To the best of the authors' knowledge, this paper is the first to present an adaptive robust algorithm based on a multivariable control structure for the voltage control of islanded ac microgrids—without prior knowledge about nominal system parameters considering the complete dynamics of IBRs and unmatched input disturbances. The main contributions of this paper are as follows.

1) A multivariable, adaptive, robust control strategy is proposed for the operation of VSC-based islanded microgrids. Unlike previous control strategies, the proposed approach is independent of system parameters. With the slightest prior knowledge and the use of online learning mechanisms, it can estimate these parameters and adjust itself to match the uncertain closed-loop system response to a selected reference dynamic model. To put it another way, the proposed control strategy can identify the unknown system parameters and simultaneously adjust control parameters. As a result, unlike most current studies—which are based on fixed controllers—no previous calculations (such as solving LMIs and algebraic Riccati equations) are needed to obtain or tune the control parameters. Typical robust control methods are too conservative. Considering possible variations in operating points, they may be subject to instability in case of changes in system parameters. It is worthy of note that the proposed control algorithm is independent of the system topology, line impedance, and load dynamics.
2) Besides the robustness against parameter variations and uncertainties, the proposed controller is robust against mismatched input disturbances. Through the complete dynamic modeling of IBRs and their output filters, mismatched input disturbances will appear in the system dynamics from the grid-side and affect system trajectories. The proposed strategy can estimate and reject these external disturbances using online adaptation rules to improve the power quality.
3) The proposed MAR algorithm allows controller designers to choose the predetermined model according to their desired priorities. For instance, the system response speed of the proposed method will be improved without increasing the system sensitivity. Still, the presented MAR method can increase the response speed via properly selecting the reference system and its properties—unlike many existing algorithms employing large feedback gains to increase it. Also, due to the lack of knowledge of the system's physical parameters, the proposed algorithm uses indirect identification to adapt the controller parameters and match the system's dynamic performance with the selected dynamic model's performance. Specifically, the dynamics of IBR units with unknown parameters will be replaced by the desired reference model. It is noteworthy that the persistent excitation condition to identify the parameters will be relaxed via the algorithm introduced.

II. Preliminaries and Problem Formulation

In this section, some essential mathematical explanations and notations are defined, which will be used throughout the manuscript. Throughout this paper, $\chi_m(s)$ stands for the left interactor matrix of a transfer function matrix like $G(s)$, which specifies the properties of the infinite zeros of $G(s)$. Readers can refer to [36] for more details. Let $\mathcal{L}$ be the Laplace transform operator. Additionally, for ease of reference and simplicity, let's define the inverse of the Laplace transform

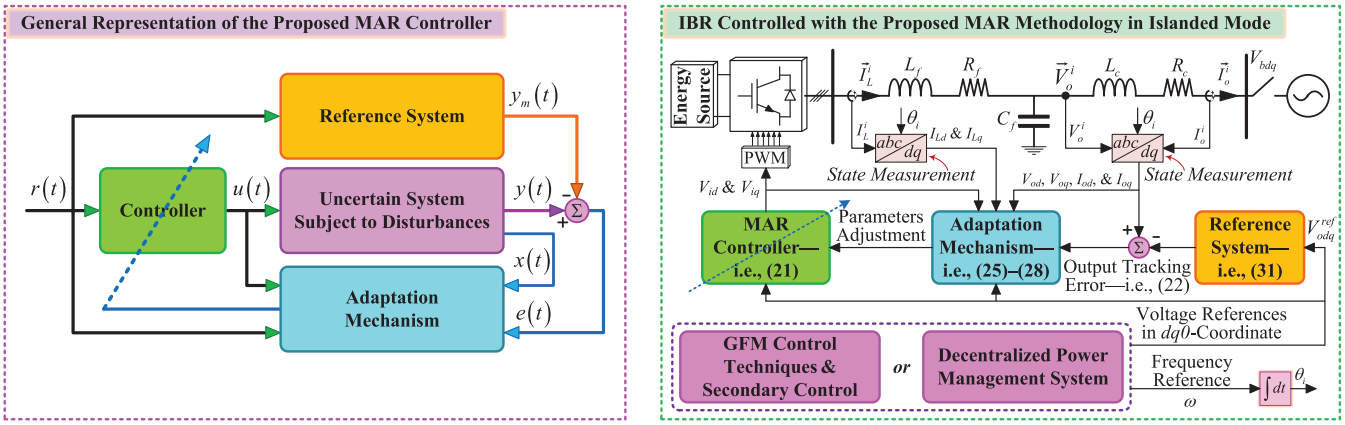

Fig. 1. Structure of the proposed MAR control (left) and the islanded IBR as an uncertain dynamic system with the proposed controller (right).

operator with $\mathcal{L}^{-1}$ such that $\mathcal{L}^{-1}\{P(s)b(s)\} \triangleq P(s)\langle b\rangle(t)$, where the outcome is a function of time, "t." In the defined operator, $P(s)$ and $b(t)$ stand for a transfer function matrix (or a filter in the frequency domain) and a continuous signal, respectively.

A. Mathematical Modeling

Consider an islanded microgrid with an arbitrary topology. A typical IBR in that is comprised of a source of electrical energy on the dc side. It is interfaced with the microgrid through a VSC, which is generally connected to the point of common coupling through an LCL filter [22]. Let $\omega = 2 \times \pi \times 60$ rad/s be the nominal frequency of the system—which can be obtained via either a GFM control method, such as the droop technique, or an internal oscillator. Thus, according to the single-line diagram shown in Fig. 1 (right side), each IBR's mathematical model in the dq-frame is expressed as

$$\begin{cases} \dot{I}_{Ld}(t) = -\dfrac{R_f}{L_f} I_{Ld}(t) + \omega I_{Lq}(t) + \dfrac{1}{L_f} V_{id}(t) - \dfrac{1}{L_f} V_{od}(t) \\ \dot{I}_{Lq}(t) = -\dfrac{R_f}{L_f} I_{Lq}(t) - \omega I_{Ld}(t) + \dfrac{1}{L_f} V_{iq}(t) - \dfrac{1}{L_f} V_{oq}(t) \\ \dot{V}_{od}(t) = \omega V_{oq}(t) + \dfrac{1}{C_f} I_{Ld}(t) - \dfrac{1}{C_f} I_{od}(t) \\ \dot{V}_{oq}(t) = -\omega V_{od}(t) + \dfrac{1}{C_f} I_{Lq}(t) - \dfrac{1}{C_f} I_{oq}(t) \\ \dot{I}_{od}(t) = -\dfrac{R_c}{L_c} I_{od}(t) + \omega I_{oq}(t) + \dfrac{1}{L_c} V_{od}(t) - \dfrac{1}{L_c} V_{bd}(t) \\ \dot{I}_{oq}(t) = -\dfrac{R_c}{L_c} I_{oq}(t) - \omega I_{od}(t) + \dfrac{1}{L_c} V_{oq}(t) - \dfrac{1}{L_c} V_{bq}(t) \end{cases} \tag{1}$$

where I_{Ldq}, V_{odq}, and I_{odq} are the dq-frame signals of the current injected to the ac-side filter, output voltage, and output current, respectively. Therefore, the state space equations of each IBR is written as

$$\begin{cases} \dot{x}(t) = Ax(t) + Bu(t) + B_w w(t) \\ y(t) = Cx(t) \end{cases} \tag{2}$$

where $x(t) = \left[I_{Ld}, I_{Lq}, V_{od}, V_{oq}, I_{od}, I_{oq}\right]^T$, $u(t) = \left[V_{id}, V_{iq}\right]^T$, $y(t) = \left[V_{od}, V_{oq}\right]^T$, and $w(t) = \left[V_{bd}, V_{bq}\right]^T$ stand for the state, input control signal, output, and mismatched input disturbance vectors, respectively. It is noteworthy that the control matrix B and the input disturbance matrix B_w are linearly independent ($B \neq \alpha B_w$), so the input disturbances affect the system states through a different input channel.

The disturbance vector $w(t)$ stands for the grid-side voltage harmonics—which should be considered in the controller design. It is assumed that the disturbance signal $w(t)$ has an upper bound which is not needed to be known. The disturbance is actually a voltage signal; therefore, it is reasonable to consider it bounded. The output LCL filter can reduce higher-order harmonics, but a proper control strategy needs to eliminate lower-order harmonics. In this regard, applying the dq-frame, the lower-order grid-side voltage harmonics (3rd, 5th, and 7th) are expressed as

$$w(t) = \begin{bmatrix} w_1(t) \\ w_2(t) \end{bmatrix} \tag{3}$$

where

$$\begin{aligned} w_1(t) &= V_{ds2}\sin(2\omega t) + V_{ds4}\sin(4\omega t) + V_{ds6}\sin(6\omega t) \\ w_2(t) &= V_{q0} + V_{qc2}\cos(2\omega t) + V_{qc4}\cos(4\omega t) \\ &\quad + V_{qc6}\cos(6\omega t). \end{aligned} \tag{4}$$

Consequently, the grid-side voltage harmonics can be presented as a summation of sinusoidal signals in the dq-frame. It is worthy of mention that the amplitudes of the disturbance signals detailed above are "*unknown*" and "*not*" required to be measured.

Although the main control objective of the studies in the literature is the same, unlike the modeling method used in [19], [22], and [25], the modeling procedure utilized in (1) does not need knowledge regarding the physical topology, loads' and/or IBRs' locations, and line impedance. Additionally, its application is not limited to a specific topology of microgrids in which loads are connected to IBRs outputs and there are only simple transmission lines between every two neighboring IBRs. The considered model is appropriate for the inner loop of GFM inverters, whether in a decentralized or hierarchical structure.

The dc side of generation units can be considered similar to the topology illustrated in Fig. 2. Accordingly, one can write

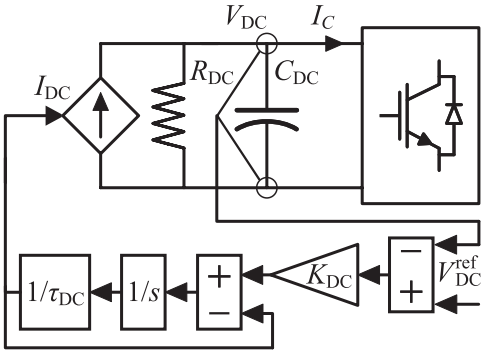

Fig. 2. DC side of the IBRs studied in this paper.

the IBRs' dc-link dynamics as follows.

$$\dot{V}_{DC}(t) = \frac{1}{C_{DC}} I_{DC}(t) - \frac{R_{DC}}{C_{DC}} V_{DC}(t) - I_C(t) \tag{5}$$

where V_{DC}, I_{DC}, I_C, R_{DC}, and C_{DC} are the voltage across the dc-link capacitance, the dc-source current, the current delivered to the converter, dc-side resistance, and dc-side capacitance, respectively. The structure of the dc side and the variables are shown in Fig. 2. I_{DC} acts as the control input of the system—which needs to be appropriately designed. The following equation is employed to emulate the dynamic response (or behavior) of the primary energy source (e.g., an energy storage system), where τ_{DC} is the time constant associated with the dynamics of the energy resource (see [37] and [38]).

$$I_{DC}(t) = \frac{1}{\tau_{DC}} \int \left(I_{DC}^{ref}(t) - I_{DC}(t) \right) dt. \tag{6}$$

The primary objective of the dc-side controller is to keep the dc voltage stable according to its reference value. In this regard, I_{DC}^{ref} is designed by a proportional controller detailed in (7).

$$I_{DC}^{ref}(t) = K_{DC}\left(V_{DC}^{ref} - V_{DC}(t) \right) \tag{7}$$

where K_{DC} is the controller gain, and V_{DC}^{ref} shows the reference value of dc voltage.

Based on the model derived earlier, the designed control system should provide three objectives, as described next. 1) The output voltage of each unit should track the reference signal (the output of the predetermined model) asymptotically, 2) the proposed controller should be able to compensate for the mismatched input disturbances and also meet the IEEE recommendations regarding the output voltage harmonic limits, 3) and the stability of the closed-loop system (considering internal signals) should be guaranteed. In order to meet these objectives, the proposed MAR control technique is designed in the following section.

Remark 1: As stated previously, the MAR control algorithm applies to the inner ac voltage control loop of IBRs operating as GFM inverters in grids. The dynamic response (or behavior) of renewable energy resources influences the dc-link dynamics—but renewables have their own control systems functioning separately from the ac-side control system. The designed control system is solely responsible for the ac-side voltage stability with a specified frequency considering parameters uncertainty and external disturbances. The stable performance of a GFM IBR on the ac side relies on the stability of its dc link. In other words, a GFM IBR stabilizes the ac-side voltage if the stability of the dc side is ensured—as the stability of the dc side is an initial assumption for the operation of GFM inverters. Still, grid-following (GFL) inverters can contribute to the stability of the dc-link voltage if they are connected to a stable ac grid with properly operating phase-locked units [39]. With this in mind, the detailed analysis of dc-link stability is out of the scope of this study; it is the primary objective of other studies where the dynamics and operation of GFL IBRs have been investigated in detail; see [40], [41], and [42].

III. Multivariable, Adaptive, Robust Control

This section designs the MAR control strategy for the primary layer of islanded microgrids; the proposed MAR control is robust against parametric uncertainties and input disturbances. Before going deep into the controller design procedure, some definitions are required.

As stated earlier, the main objective is to make the output of the uncertain system to track the output of the selected reference system. In other words, an arbitrary predetermined model to achieve our desired dynamic performance replaces the actual dynamics (stable or unstable ones) of IBR units with unknown parameters. To this end, the output voltage of each IBR should track $y_m(t)$, i.e.,

$$y_m(t) = G_m(s)\langle r \rangle(t), \tag{8}$$

where $r(t) \in \Re^2$ and $G_m(s) \in \Re^{2\times 2}$ are the reference signal and the reference dynamics, respectively; for the meaning of the $G_m(s)\langle r \rangle(t)$ expression—or generally speaking, the mathematical operator of $P(s)\langle b \rangle(t)$—readers are referred to the preliminaries described at the beginning of Section II.

In (8), the reference system is chosen to be $G_m(s) = \chi_m^{-1}(s)$, where $\chi_m(s)$ is the left interactor matrix of $G(s) = C(sI - A)^{-1}B$. The high-frequency gain matrix associated with $\chi_m(s)$ is defined as $K_H = \lim_{s\to\infty} \chi_m(s)G(s)$. It should be noted that if the left interactor matrix $\chi_m(s)$ is diagonal, the high-frequency gain matrix will also be diagonal.

Assumption 1: $G(s)$ is full rank such that K_H is non-singular.

Lemma 1: if the matrix of

$$K_G = \begin{bmatrix} C_1 A^{\eta_1 - 1} B \\ \vdots \\ C_1 A^{\eta_M - 1} B \end{bmatrix} \in \Re^{M\times M} \tag{9}$$

exists for a specific relative degree like $\eta_i > 0$ (for $i = 1, 2, \ldots, M$) and is non-singular, it is concluded that the left interactor matrix is diagonal such that $\chi_m(s) = diag(h_1(s), \ldots, h_M(s))$ and $K_H = K_G$ [36]. $h_i(s) = s^{\eta_1} + b_{i\eta_1 - 1}s^{\eta_1 - 1} + \ldots + b_{i1}s + b_{i0}$ are arbitrary stable polynomials.

Assumption 2: The zeros of $G(s)$ are stable, and there exists a matrix like $V_H \in \Re^{2\times 2}$ such that

$$K_H^T V_H^{-1} = \Sigma_P = \Sigma_P^T > 0. \tag{10}$$

TABLE I
TEST SYSTEM'S PARAMETERS

Description	IBR #1 & IBR #2	IBR #3 & IBR #4
$\mathbf{R_c}$	$0.03\,\Omega$	$0.032\,\Omega$
$\mathbf{L_c}$	$0.35\,\mathrm{mH}$	$0.37\,\mathrm{mH}$
$\mathbf{L_f}$	$1.35\,\mathrm{mH}$	$1.35\,\mathrm{mH}$
$\mathbf{R_f}$	$0.1\,\Omega$	$0.1\,\Omega$
$\mathbf{C_f}$	$50\,\mu\mathrm{F}$	$50\,\mu\mathrm{F}$
$\mathbf{C_{DC}}$	$0.001\,\mathrm{F}$	$0.001\,\mathrm{F}$
$\mathbf{R_{DC}}$	$8\,\Omega$	$8\,\Omega$
τ_{DC}	$50\,\mathrm{ms}$	$50\,\mathrm{ms}$
PWM switching frequency	$8.10\,\mathrm{kHz}$	
Sampling frequency	$25\,\mathrm{kHz}$	
Loads	**Loads 1 & 2**	**Loads 3 & 4**
	$6\,\mathrm{kW}+2\,\mathrm{kvar}$	$6.5\,\mathrm{kW}+2\,\mathrm{kvar}$
Lines	**Lines 1, 2, 4, & 5**	**Lines 3 & 6**
	$0.12\,\Omega+0.418\,\mathrm{mH}$	$0.35\,\Omega+1.847\,\mathrm{mH}$

By using *Lemma* 1, the high-frequency gain matrix is calculated with $\eta_i = 2$ as

$$CAB = \begin{bmatrix} \dfrac{1}{C_f L_f} & 0 \\ 0 & \dfrac{1}{C_f L_f} \end{bmatrix}. \tag{11}$$

It is observed that K_H is always diagonal and full rank independent of system parameters. According to the dynamic models in [17], and considering the parameters in Table I, it is concluded that the zeros of $G(s)$ are stable. Finally, considering the properties of the high-frequency gain matrix, V_H can be chosen as $V_H = \Sigma_1 = \Sigma_1^T$ to satisfy (10).

A. Nominal Control Algorithm

This part presents the nominal structure of the proposed controller in order to determine the algebraic feasibility of the selected algorithm. Note that in this part, it is assumed that the system's parameters are entirely known. As a result, just the algebraic feasibility of the nominal controller will be investigated. After investigating the feasibility of the nominal structure, in the next section assuming that the nominal parameters are not known, the online adaptation rules will be used to construct the actual controller. The nominal control algorithm is presented as

$$u(t) = K_1^* x(t) + K_2^* r(t) + K_3^*(t) \tag{12}$$

where $K_1^* \in \Re^{2\times 6}$ and $K_2^* \in \Re^{2\times 2}$ are nominal feedback gains (not functions of time) to track the reference signal, and $K_3^*(t) \in \Re^2$ is the disturbance rejection term; $K_3^*(t)$ is a function of time, "t," as indicated in parentheses.

Theorem 1: The output of the system in (2) tracks the reference signal $y_m(t) = G_m(s)\langle r\rangle(t)$ asymptotically in the presence of the disturbance vector $w(t)$, using the nominal control algorithm (12) such that $\lim_{t\to\infty}(y(t) - y_m(t)) = 0$.

Proof: Consider the output of the system (2) as $y(t) = \begin{bmatrix} y_1(t) & y_2(t)\end{bmatrix}^T$. Let's define the control signal as $u(t) = K_H^{-1}\vartheta(t)$ with $\vartheta(t) = [\vartheta_1(t)\ \ \vartheta_2(t)]^T$ and $K_{hi} = C_i A^{\eta_i - 1}B$ for $i = 1, 2$. According to the relative degree of the system, the second derivative of the output is written as

$$\ddot{y}_i(t) = C_i A^2 x(t) + C_i A B u(t) + C_i A B_w w(t) + C_i A B_w \dot{w}(t). \tag{13}$$

Substituting the control signal $u(t)$ into (13) results in

$$\ddot{y}_i(t) = C_i A^2 x(t) + \vartheta_i(t) + C_i A B_w w(t) + C_i A B_w \dot{w}(t). \tag{14}$$

Consider the auxiliary control signal $\vartheta_i(t)$ defined as

$$\vartheta_i(t) = -C_i A^2 x(t) - b_{i1}\dot{y}_i(t) - b_{i0} y(t) - C_i A B_w w(t) - C_i B_w \dot{w}(t) + r_i(t). \tag{15}$$

Therefore, (14) is written as

$$\ddot{y}_i(t) + b_{i1}\dot{y}_i(t) + b_{i0} y(t) = r_i(t). \tag{16}$$

As a result,

$$y_i(s) = \frac{1}{h_i(s)} r_i(s), \quad y(s) = G_m(s) r(s) \tag{17}$$

where the reference system $G_m(s)$ is the inverse of left interactor matrix. The auxiliary signal $\vartheta_i(t)$ is considered as $\vartheta(t) = \bar{K}x(t) + \bar{K}_1\omega(t) + \bar{K}_2\dot{\omega}(t) + r(t)$ with

$$\begin{cases} \bar{K} = \begin{bmatrix}\bar{k}_1^T & \bar{k}_2^T\end{bmatrix}^T \\ \bar{k}_i^T = -C_i A^2 - b_{i1} C_i A - b_{i0} C_i \end{cases}, \begin{cases} \bar{K}_1 = \begin{bmatrix}\bar{k}_{11}^T & \bar{k}_{12}^T\end{bmatrix}^T \\ \bar{k}_{1i} = -C_i A B_w \end{cases}$$
$$\begin{cases} \bar{K}_2 = \begin{bmatrix}\bar{k}_{21}^T & \bar{k}_{22}^T\end{bmatrix}^T \\ \bar{k}_{2i} = -C_i B_w. \end{cases} \tag{18}$$

Thus, the nominal control signal is expressed as $u(t) = K_H^{-1}\big[\bar{K}x(t) + \bar{K}_1 w(t) + \bar{K}_2\dot{w}(t) + r(t)\big]$ with the nominal gains of $K_1^* = K_H^{-1}\bar{K}$, $K_2^* = K_H^{-1}$, and $K_3^*(t) = K_H^{-1}\big[\bar{K}_1 w(t) + \bar{K}_2\dot{w}(t)\big]$. It is observed that the nominal control signal (12) causes the output to track the reference signal asymptotically in the presence of unmatched input disturbances. This observation concludes the proof. ■

B. Matching Condition

From the previous subsection, it is concluded that for the condition of

$$G_m(s)K_2^{*-1}K_3^*(s) + C\Big(sI - A - BK_1^{*T}\Big)^{-1} B_w w(s) = 0$$
$$C\Big(sI - A - BK_1^{*T}\Big)^{-1} BK_2^{*T} = G_m(s), \tag{19}$$

there exist non-singular matrices $K_1^* \in \Re^{2\times 6}$, $K_2^* \in \Re^{2\times 2}$, and disturbance rejection term $K_3^*(t) \in \Re^2$ to satisfy (19). The input disturbances are summation of some sinusoidal signals, so their derivatives are well defined, and one can parameterize them [31]. Consider $w(t) = \Psi^{*T} g(t)$ and $\dot{w}(t) = \tilde{\Psi}^{*T} g(t)$ where $\Psi^* \in \Re^{8\times 2}$, $\tilde{\Psi}^* \in \Re^{8\times 2}$, and $g(t) \in \Re^8$ are parameterization terms associated with $w(t)$ and $\dot{w}(t)$.

Let's assume that $g(t)$ is a continuous function. Therefore, the disturbance rejection term $K_3^*(t)$ is parameterized as

$$K_3^*(t) = K_H^{-1}\left[\bar{K}_1\Psi^* g(t) + \bar{K}_2\tilde{\Psi}^* g(t)\right] = \varphi_3^* g(t)$$
$$\varphi_3^* = K_H^{-1}\left[\bar{K}_1\Psi^* + \bar{K}_2\tilde{\Psi}^*\right] \in \Re^{2\times 8}. \quad (20)$$

Remark 2: It should be emphasized that we just know the structure of disturbance signal $w(t)$ and its derivative $\dot{w}(t)$, not their actual value. According to the sinusoidal structure of the disturbance signal in (3), the structure of the first derivative of the signal can be obtained from $w(t)$. Therefore, the adaptation mechanism discussed in the next subsection can estimate φ_3^* in order to compensate for the disturbance term.

C. Proposed MAR Algorithm

Similar to the nominal design in (12), the proposed MAR algorithm is expressed as

$$u(t) = K_1(t)x(t) + K_2(t)r(t) + K_3(t) \quad (21)$$

where $K_1(t)$, $K_2(t)$, and $K_3(t)$ are the estimates of the nominal parameters. In the following, online adaptation rules will be obtained in order to estimate the nominal parameters of the closed-loop system.

D. Tracking and Estimation Errors

The construction of error signals is one of the critical stages in adaptive control systems. The first step is to obtain the output tracking error. According to the conditions in (19), the output tracking error is written as

$$e(t) = y(t) - y_m(t)$$
$$= G_m(s)K_2^{*-1}\left\langle\tilde{\gamma}^T\kappa\right\rangle(t) + Ce^{\left(A+BK_1^{*T}\right)t}x(t) \quad (22)$$

where $\tilde{\gamma}(t) = \gamma(t) - \gamma^*$ is the parameter estimation error, and for $\kappa(t) \in \Re^{16}$, γ^{*T}, and $\gamma^T(t) \in \Re^{2\times 16}$, we have

$$\kappa(t) = \left[x^T(t)\ r^T(t)\ g^T(t)\right]^T$$
$$\gamma^{*T} = \left[K_1^* \quad K_2^* \quad \varphi_3^*\right]$$
$$\gamma^T(t) = \left[K_1(t) \quad K_2(t) \quad \varphi_3(t)\right]. \quad (23)$$

As the exponential term in (22) decays to zero, the output estimation error is rewritten as

$$e(t) = G_m(s)K_2{}^{*-1}\left\langle\tilde{\gamma}^T\kappa\right\rangle(t), \quad (24)$$

which is completely measurable.

In the next step, it is required to construct the estimation error. In this regard, consider $p(s) = \frac{1}{q(s)}$ with $q(s) = s^2 + q_1 s + q_0$ as an arbitrary stable polynomial. As a result, the estimation error $\delta(t)$ is defined as

$$\delta(t) = \chi_m(s)p(s)\langle e\rangle(t) + \Gamma(t)\lambda(t) \quad (25)$$

where $\Gamma(t)$ is the estimation of the high-frequency gain matrix K_H. Let Γ^* be the nominal value of K_H. As a result, the estimation error of high-frequency gain matrix is defined as $\tilde{\Gamma}(t) = \Gamma(t) - \Gamma^*$. In the following, let's define $\lambda(t)$ and $\sigma(t)$ as

$$\lambda(t) = \gamma^T(t)\sigma(t) - p(s)\langle u\rangle(t)$$
$$\sigma(t) = p(s)\langle\kappa\rangle(t). \quad (26)$$

Using (24), it is concluded that

$$\delta(t) = \Gamma^*\tilde{\gamma}(t)\sigma(t) + \tilde{\Gamma}(t)\lambda(t). \quad (27)$$

It is observed that the estimation error $\delta(t)$, $\lambda(t)$, and $\sigma(t)$ are all based on measurable signals.

Remark 3: Although the structure of the controller proposed in (21) is linear, it is classified as a nonlinear controller. The existence of time varying adaptive parameters $K_1(t)$, $K_2(t)$, and $K_3(t)$ that are functions of system states and measured errors, such as $\kappa(t)$ and $\delta(t)$, makes the control algorithm as well as the closed-loop system nonlinear.

E. Online Adaptation Rules

This section constructs the online adaptation rules required to estimate the unknown parameters using measurable signals. In this regard, it is assumed that $K_1(t)$, $K_2(t)$, and $K_3(t)$ are unknown, so it is needed to identify them using measurable signals. Let's define $\Sigma_1 = \Sigma_1^T > 0$ and $\Sigma_2 = \Sigma_2^T > 0$ as some arbitrary design parameters which are used to tune the adaptation speed. Thus, the adaptive laws are written as

$$\dot{\gamma}^T(t) = -\frac{\Sigma_1\delta(t)\sigma^T(t)}{n^2(t)}$$
$$\dot{\Gamma}(t) = -\frac{\Sigma_2\delta(t)\lambda^T(t)}{n^2(t)} \quad (28)$$

where $n^2(t) = 1 + \sigma^T(t)\sigma(t) + \lambda^T(t)\lambda(t)$.

Lemma 2: Using the online adaptation rules obtained in (28), one can guarantee that $\gamma(t), \Gamma(t) \in L^\infty$ and $\frac{\delta(t)}{n(t)}, \dot{\gamma}(t), \dot{\Gamma}(t) \in L^2 \cap L^\infty$.

Proof: Consider the energy function of

$$V(t) = \frac{1}{2}\left[tr\left(K_H\tilde{\gamma}^T\Sigma_1^{-1}\tilde{\gamma}\right) + tr\left(\tilde{\Gamma}^T\Sigma_2^{-1}\tilde{\Gamma}\right)\right]. \quad (29)$$

Let's define $K_H = k_h I$ for $k_h > 0$. Considering the fact that $trace\left(xy^T\right) = x^T y$ for two arbitrary vectors $x, y \in \Re^n$, the time derivative of the energy function is written as

$$\dot{V}(t) = -\frac{\delta^T(t)\delta(t)}{n^2(t)} \le 0. \quad (30)$$

As a result, one deduces that $\gamma(t) \in L^\infty, \Gamma(t) \in L^\infty$, $\frac{\delta(t)}{n(t)} \in L^2 \cap L^\infty$, $\dot{\gamma}(t) \in L^2 \cap L^\infty$, and $\dot{\Gamma}(t) \in L^2 \cap L^\infty$—thereby concluding the proof.

Note: Given the length of complementary details regarding the stability analysis and page limitations, more details can be found in the 9th chapter of [43]. ■

Remark 4: In summary, the main objective of the presented MAR control algorithm is to conform the dynamical behavior of the system (with unknown parameters) to an arbitrary reference system. Considering designers' priorities, it is first required to select a dynamical model (usually a decoupled system with fast dynamics). This model demonstrates the desired dynamics that replace the original dynamics of IBR

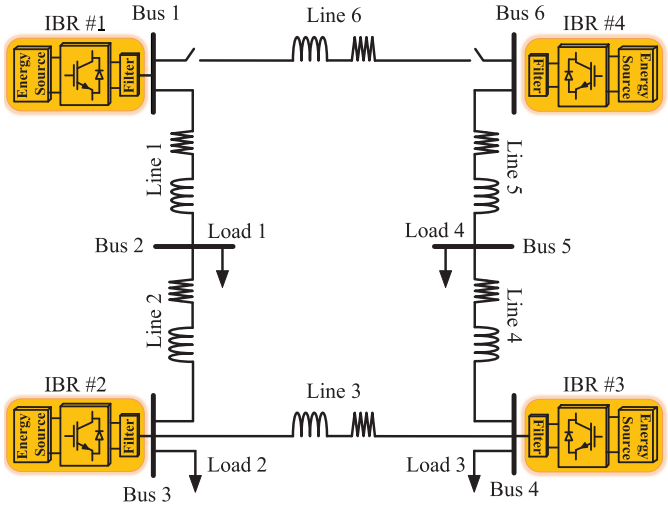

Fig. 3. Single-line diagram of the test microgrid.

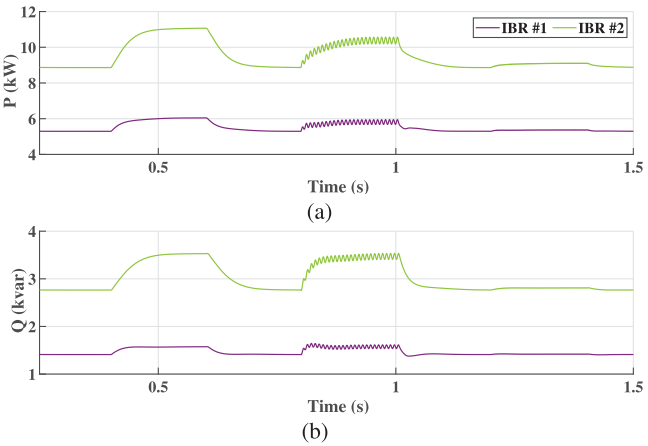

Fig. 4. Scenarios 1, 2, and 3 (Step Load Change, Short-Circuit Fault, and Nonlinear Load Connection): IBRs #1's and #2's output (a) active power and (b) reactive power.

units. Then, it is needed to form the online adaptation rules in (28) using available measurements without tuning or obtaining any control parameters through solving LMIs or any other algebraic equation. All that is needed is to choose adaptation gains that only affect the adaptation speed of the control parameters [$K_1(t)$, $K_2(t)$, and $K_3(t)$] to their nominal values. The designed control system regulates the amplitude of IBRs terminal voltages with a specific frequency; it also guarantees the stability of all other state variables regardless of parameter uncertainty and grid-side disturbances with prescribed performance. As a result, the voltage and frequency stability of the system is ensured as long as the designed control system has a solid performance.

The proposed structure uses an online adaptation mechanism to identify unknown parameters and then adapt control parameters according to the physical characteristic of the unknown system. In fact, unlike offline methods, which rely on existing datasets to form a control structure, this method can be applied to an IBR without the need for prior measured data collection, so it uses posterior information for the adjustment. Additionally, the online adaptation mechanism allows the control system to adjust itself to possible changes in system parameters in real time during different contingencies.

IV. Simulation Results

This section verifies the proposed MAR algorithm through carrying out simulations of the test microgrid system (see Fig. 3) in MATLAB/SimPowerSystems environment. The parameters of the system under study are presented in Table I—which is just employed to simulate a test microgrid system—otherwise, these parameters have "*not*" been used at any stage of the controller design process. The electrical loads are constant impedance type. The loads' power varies with the square of their terminal voltage magnitude. The control algorithm used in this study does not rely on the loads' types and their characteristics; its performance does not depend on them either. According to the dynamic model in (1) and (2), IBRs' output current is one of the state variables—which includes the power losses and the currents supplying loads—but there is no constraint on the type of loads they are feeding. Besides, it is worth noting that the proposed control scheme is completely independent of the system's size and topology and the number of IBRs. As a result, it can be applied to a microgrid with arbitrary size and physical topology. The nominal frequency of the system is 60 Hz, and the voltage reference is chosen to be $V_{od}^{\text{ref}} = 208\sqrt{2}$ and $V_{oq}^{\text{ref}} = 0$ for all IBRs. GFM control methods or decentralized management systems provide these reference values for the inner control loop. The nominal dc voltage is set to $V_{\text{DC}}^{\text{ref}} = 900$, and the proportional gain is chosen to be $K_{\text{DC}} = 150$. The reference system is selected as any arbitrary stable 2×2 transfer function matrix with $\eta = 2$. Therefore, the predetermined dynamics of interest are chosen to be

$$G_m(s) = \begin{bmatrix} \dfrac{9900}{(s+90)(s+110)} & 0 \\ 0 & \dfrac{9900}{(s+90)(s+110)} \end{bmatrix}. \quad (31)$$

Adaptation gains and the design filter are also chosen to be $\Sigma_1 = \Sigma_2 = 90$ and $q(s) = (s+250)(s+300)$, respectively. It should be noted that the predetermined system's parameters (e.g., transfer function's poles) can be arbitrarily selected. Therefore, the closed-loop system's speed and performance can be tuned "*without*" changing the controller's gain, and hence increasing the closed-loop system's sensitivity.

The simulation studies are carried out through two different scenarios. Besides, the performance of the proposed MAR algorithm is compared with the robust control method in [18].

A. Scenario 1: Step Load Change

The first scenario deals with the system's robustness against a step load change. In this regard, the test microgrid system starts its operation in islanded mode at $t = 0$ s. At $t = 0.4$ s, Load 2 is increased by 50%, and at $t = 0.6$ s is decreased to its nominal value. Fig. 4 (up to $t = 0.8$ s) shows Scenario 1 detailed above. Also, as Fig. 5 shows the voltage and current signals, IBR #2 responds well to this disturbance, and its output voltage remains in a stable region without having any noticeable fluctuations.

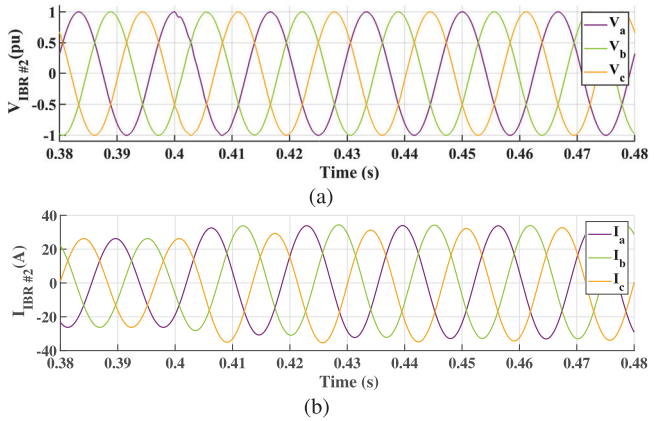

Fig. 5. Scenario 1 (Step Load Change): IBR #2's instantaneous three-phase (a) voltages and (b) currents.

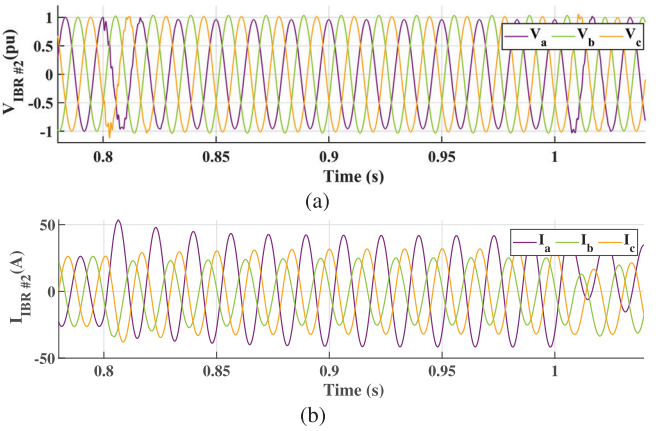

Fig. 6. Scenario 2 (Short-Circuit Fault): IBR #2's instantaneous three-phase (a) voltages and (b) currents.

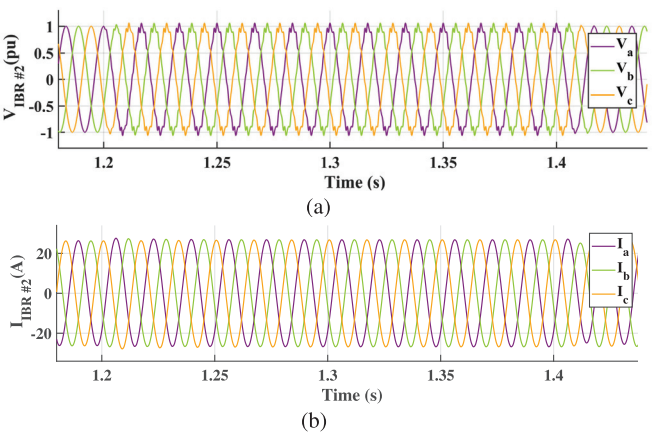

Fig. 7. Scenario 3 (Nonlinear Load Connection): IBR #2's instantaneous three-phase (a) voltages and (b) currents.

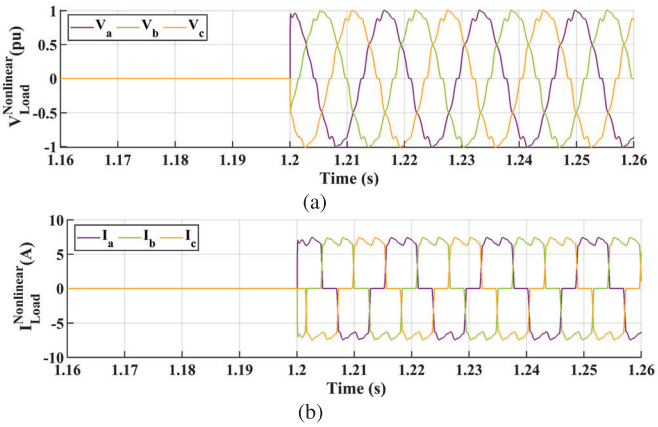

Fig. 8. Scenario 3 (Nonlinear Load Connection): Nonlinear load's instantaneous three-phase (a) voltages and (b) currents.

B. Scenario 2: Short-Circuit Fault

The objective of this case study is to evaluate the performance of the proposed control method with respect to a sudden short-circuit fault. In this regard, a single-phase short-circuit fault (phase a) with a resistance of $R_{\text{slg}} = 0.01\Omega$ strikes Bus 4 at $t = 0.8$ s and is next cleared at $t = 1$ s. This event causes some fluctuations in IBRs' output currents. Nevertheless, the output voltages show minor, negligible oscillations and remain stable in response to this fault. Fig. 4 (from $t = 0.8$ s to $t = 1.2$ s) shows active and reactive powers associated with Scenario 2 detailed above.

Fig. 6 presents IBR #2's responses. Its results show that after a short transient, the output current of the unit converges to its steady-state value. As expected, the tracking performance of the output voltage is completely acceptable and shows the robustness of the closed-loop system.

C. Scenario 3: Nonlinear Load Connection

In this scenario, the performance of the proposed control scheme is evaluated by the connection of a 3-phase nonlinear harmonic load, a six-pulse diode rectifier, to the test system. To this end, a 3-phase nonlinear harmonic load with $R = 40\,\Omega$ and $L = 0.01$ mH is connected to Bus 4 at $t = 1.2$ s and then disconnected at $t = 1.4$ s. The responses of the output voltage and current of IBR #2 are plotted in Fig. 7. Additionally, the instantaneous voltages and currents of the nonlinear load can be seen in Fig. 8. The nonlinear load draws a non-sinusoidal current that does not follow the characteristic of its voltage waveform. Although nonlinear loads generate harmonics intensively, the voltage regulation is well achieved, and there is not any considerable fluctuation in response to the connection of the nonlinear load.

Consequently, the proposed MAR method is able to guarantee a robust performance of the closed-loop system during the scenarios mentioned above. In this regard, Fig. 10 shows the *dq*-components of IBRs' output voltages. Also, Figs. 4(a) and (b) shows the instantaneous active and reactive powers of IBRs #1 and #2, respectively. According to the IEEE recommendations, the maximum allowable voltage THD is 5%. In this regard, Fig. 9(a) depicts IBR #2's voltage THD, for example. The results confirm that the voltage THD of IBR #2 does not exceed its maximum threshold except for transients. The voltage THD results affirm the robustness of the designed control system against grid-side disturbances, which is obtained through the online adaptation mechanism to estimate the unmatched input disturbances. Also, the performance of the proposed method in tracking the reference signals can be investigated using the voltage tracking error plotted in Fig. 9(b). Moreover, to examine the performance of the proposed method from another perspective, the evaluation of the IBRs trajectories (V_{od}, V_{oq}, and also output tracking

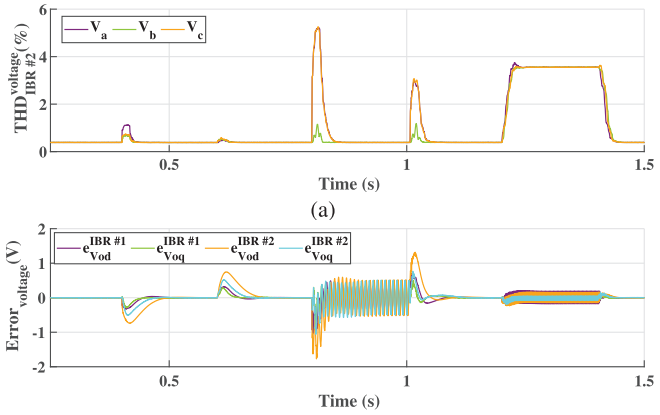

Fig. 9. Scenarios 1, 2, and 3 (Step Load Change, Short-Circuit Fault, and Nonlinear Load Connection): (a) Voltage THD of IBR #2 and (b) the voltage tracking errors of IBRs #1 and #2.

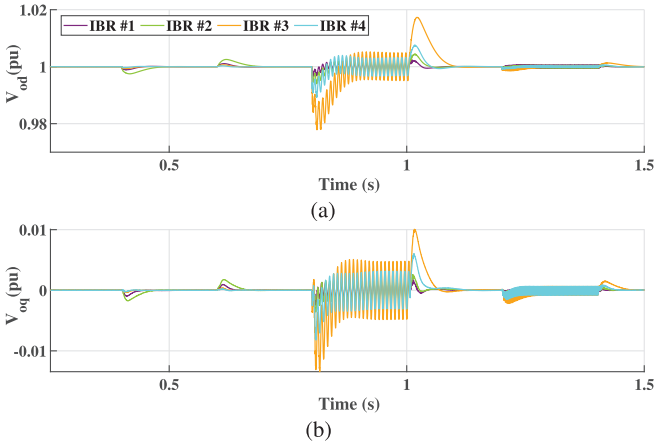

Fig. 10. Scenarios 1, 2, and 3 (Step Load Change, Short-Circuit Fault, and Nonlinear Load Connection): Performance of the (a) d and (b) q components of the output voltages.

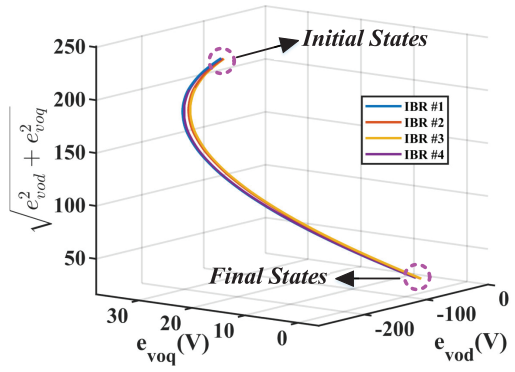

Fig. 11. Trajectories of voltage tracking errors.

errors) are displayed in Figs. 11 and 12 for all the simulation scenarios. They reveal that the output voltages' dq-components have practically reached their reference values (starting from zero initial condition). As a result, the tracking errors have converged to a bounded range around zero.

D. Comparisons With Results of Sliding Mode Control

For the last case of simulation studies, the performance of the introduced method is compared with the presented control

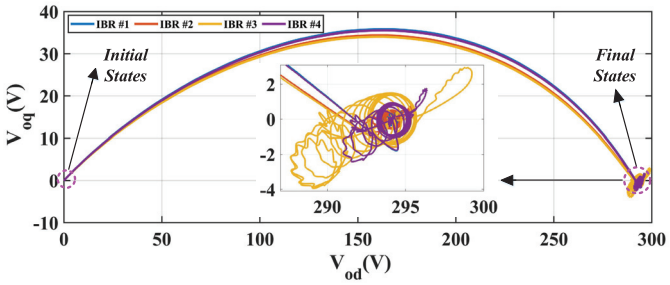

Fig. 12. Output voltage trajectories of IBRs.

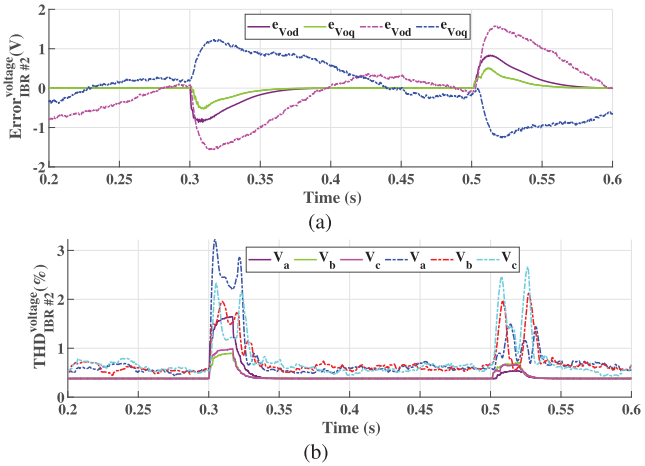

Fig. 13. Results produced by the controller in [18] for comparisons: (a) Voltage tracking errors and (b) voltage THD of IBR #2—solid lines and dash-dotted ones are associated with the proposed method and the method in [18], respectively.

method in [18]. The authors in [18] have presented a robust control structure for islanded ac microgrids using two cascaded control loops. The inner loop in this method is based on an integral sliding mode control. The outer loop uses a mixed H_2/H_∞ controller. The design procedure of both control loops requires knowledge of the system's physical parameters. In addition to being overly conservative, it is necessary to solve LMIs to obtain the outer loop control parameters for different operation conditions. Nevertheless, the proposed method does not need any prior algebraic calculations. Indeed, it uses online learning mechanisms to identify the physical parameters and adjust the control system parameters.

In this regard, the performance of the algorithm selected is compared with that of the proposed method using the first scenario of the simulation studies. To this end, Load 2 encounters 50% and is then decreased at $t = 0.3$ s and $t = 0.5$ s, respectively. Fig. 13 displays the tracking errors and voltage THDs of both methods. As a result, it is concluded that the proposed method has a solid tracking performance and disturbance rejection capability compared with the chosen robust method.

V. Experimental Results

The test rig depicted in Fig. 14 is deployed to conduct experimental examinations related to IBR #2 in the Simulation Results section. It is built by SEMIKRON intelligent power modules using insulated gate bipolar transistors (IGBTs) (based on "SKM 50 GB 123 D" modules). Besides,

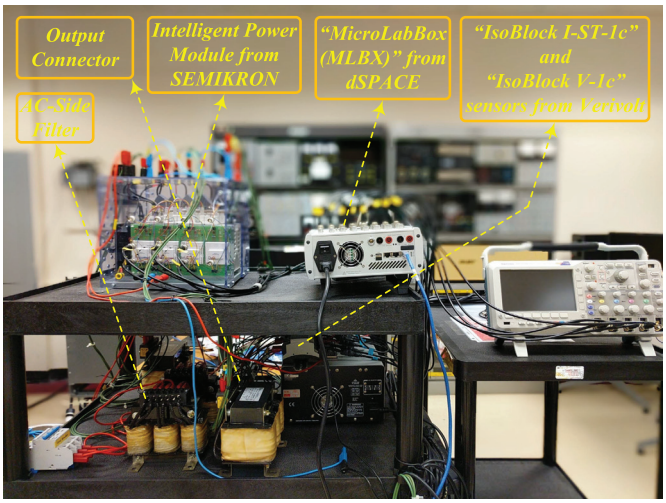

Fig. 14. Test rig used in the experiments and details of IBR—housed in the Laboratory for Advanced Power and Energy Systems (LAPES) at Georgia Southern University—where experiments have been conducted.

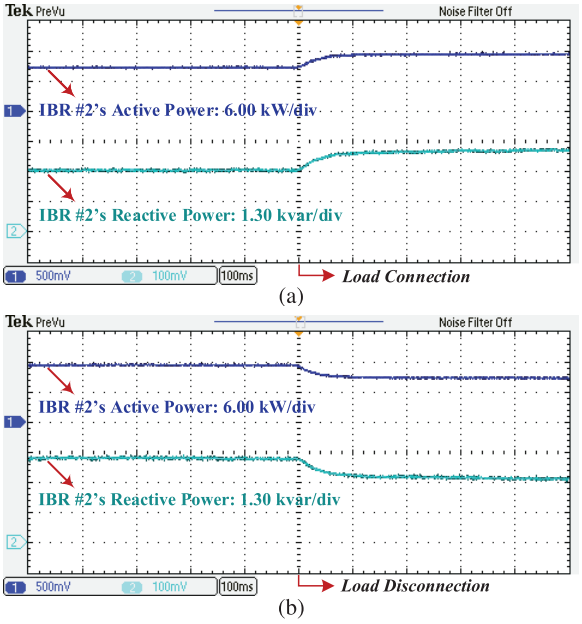

Fig. 15. Experimental results (with the 100 ms/div horizontal axis) associated with simulation results related to IBR #2 shown in Figs. 4(a) and (b) (for the time frame from $t = 0.3$ s to $t = 1.0$ s): (a) Load connection test in which active power and reactive power are shown by traces in black and cyan with 6.00 kW/div and 1.30 kvar/div (their "actual" pu values for active and reaction power signals are noted in the left-bottom corner of the figures), respectively; and (b) load disconnection test with the signal information detailed in Fig. 15(a).

SEMIKRON "SKHI 21A (R)" gate drives and protection circuitry are employed to make the converter functional. Verivolt "IsoBlock I-ST-1c"/"IsoBlock V-1c" current/voltage sensors are hooked to digital inputs to measure the currents and the voltages, respectively. dSPACE "MicroLabBox (MLBX)" using a real-time processor and field-programmable gate arrays (commonly known as FPGAs) and benefiting from PWM signals (generated by digital inputs/outputs) connects the VSC under test to the printed circuit boards of the measurement and drive circuits.

Furthermore, all of the parameters of the setup deployed are similar to those of simulations, as stated in Table I. Therefore,

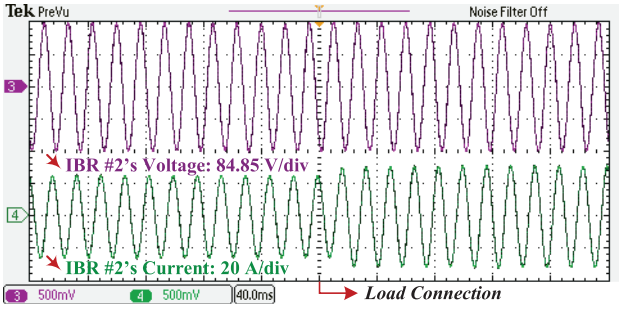

Fig. 16. Experimental results (with the 40 ms/div horizontal axis) associated with the simulation results related to IBR #2 shown in Fig. 5; load connection test in which active power and reactive power are shown by traces in magenta and lawn green with 84.85 V/div [(for the peak value)—or equivalently 60 V/div (for the rms value)]—and 20 A/div (for the peak value), respectively—their "actual" per unit (pu) values for voltage and current signals are noted in the left-bottom corner of the figure.

the comparison between simulation and experiment results is feasible. In this regard, Fig. 15 replicates the time frame from $t = 0.3$ s to $t = 1.0$ s in Fig. 4, and Fig. 16 reproduces Fig. 5. Comparing Fig. 15 with Fig. 4 and Fig. 16 with Fig. 5 reveals that simulations and experiments match well with each other. The agreement on time responses demonstrated in simulations and experimental results, which are altogether consistent, reveal the effectiveness of the proposed control methodology employed in IBR #2.

VI. Conclusion

A multivariable, adaptive, robust control method for the islanded operation of ac microgrids has been proposed and studied in this paper. The presented method provides a stable and robust performance for autonomous microgrids and is independent of microgrids' load dynamics, size, and topology. What is more, there is no need to know the nominal values of the system's physical parameters to design the controller. Online adaptation and estimation mechanisms identify the system's physical parameters; the controller parameters are tuned according to an arbitrary predetermined model of interest chosen by the controller designer. Compared with other control methods, the proposed strategy is less conservative; unlike conventional robust algorithms, there is no need to do any mathematical calculations or solve algebraic equations to adjust the control parameters. The MAR controller has a simple structure compared with high-order robust methods, is less conservative, and, more importantly, does not need to be re-tuned over time. Furthermore, it gives the system operator a large degree of freedom to select an ideal dynamic for the closed-loop system to imitate. The proposed control strategy can be applied to the inner voltage controller of GFM inverters for the reliable operation of isolated microgrids. Finally, various comparative simulations and experiments have been employed to verify the accuracy and validity of the proposed method in response to different scenarios and disturbances. Future work includes employing an optimal criterion for choosing adaptation gains to be addressed as the potential development.

References

[1] M. Farrokhabadi et al., "Microgrid stability definitions, analysis, and examples," *IEEE Trans. Power Syst.*, vol. 35, no. 1, pp. 13–29, Jan. 2020.

[2] R. Pérez-Ibacache, C. A. Silva, and A. Yazdani, "Linear state-feedback primary control for enhanced dynamic response of AC microgrids," *IEEE Trans. Smart Grid*, vol. 10, no. 3, pp. 3149–3161, May 2019.

[3] Z. Wang, Y. Yu, W. Gao, M. Davari, and C. Deng, "Adaptive, optimal, virtual synchronous generator control of three-phase grid-connected inverters under different grid conditions—An adaptive dynamic programming approach," *IEEE Trans. Ind. Informat.*, vol. 18, no. 11, pp. 7388–7399, Nov. 2022, doi: 10.1109/TII.2021.3138893.

[4] Y. Huang, Q. Sun, Y. Li, H. Zhang, and Z. Chen, "Adaptive-discretization based dynamic optimal energy flow for the heat-electricity integrated energy systems with hybrid AC/DC power sources," *IEEE Trans. Autom. Sci. Eng.*, early access, Jul. 12, 2022, doi: 10.1109/TASE.2022.3188277.

[5] C. Zhai, H. D. Nguyen, and X. Zong, "Dynamic security assessment of small-signal stability for power grids using windowed online Gaussian process," *IEEE Trans. Autom. Sci. Eng.*, early access, May 12, 2022, doi: 10.1109/TASE.2022.3173368.

[6] L.-N. Liu and G.-H. Yang, "Distributed fixed-time optimal resource management for microgrids," *IEEE Trans. Automat. Sci. Eng.*, vol. 20, no. 1, pp. 404–412, Jan. 2023, doi: 10.1109/TASE.2022.3155163.

[7] M. Davari, W. Gao, Z.-P. Jiang, and F. L. Lewis, "An optimal primary frequency control based on adaptive dynamic programming for islanded modernized microgrids," *IEEE Trans. Autom. Sci. Eng.*, vol. 18, no. 3, pp. 1109–1121, Jul. 2021.

[8] A. La Bella, S. R. Cominesi, C. Sandroni, and R. Scattolini, "Hierarchical predictive control of microgrids in islanded operation," *IEEE Trans. Autom. Sci. Eng.*, vol. 14, no. 2, pp. 536–546, Apr. 2017.

[9] S. M. Azimi and S. Lotfifard, "A nonlinear controller design for power conversion units in islanded micro-grids using interconnection and damping assignment tracking control," *IEEE Trans. Sustain. Energy*, vol. 12, no. 1, pp. 284–292, Jan. 2021.

[10] M. Raeispour, H. Atrianfar, M. Davari, and G. B. Gharehpetian, "Fault-tolerant, distributed control for emerging, VSC-based, islanded microgrids—An approach based on simultaneous passive fault detection," *IEEE Access*, vol. 10, pp. 10995–11010, 2022.

[11] U. Bose, S. K. Chattopadhyay, C. Chakraborty, and B. Pal, "A novel method of frequency regulation in microgrid," *IEEE Trans. Ind. Appl.*, vol. 55, no. 1, pp. 111–121, Jan. 2019.

[12] Y. Lin et al., "Research roadmap on grid-forming inverters," Nat. Renew. Energy Lab. (NREL), Golden, CO, USA, Tech. Rep. NREL/TP-5D00-73476, 2020.

[13] M. Raeispour, H. Atrianfar, H. R. Baghaee, and G. B. Gharehpetian, "Robust sliding mode and mixed H_2/H_∞ output feedback primary control of AC microgrids," *IEEE Syst. J.*, vol. 15, no. 2, pp. 2420–2431, Jun. 2021.

[14] S. K. Sahoo, A. K. Sinha, and N. K. Kishore, "Control techniques in AC, DC, and hybrid AC–DC microgrid: A review," *IEEE J. Emerg. Sel. Topics Power Electron.*, vol. 6, no. 2, pp. 738–759, Jun. 2018.

[15] H. Karimi, M. Karimi-Ghartemani, and K. Sheshyekani, "Robust control of three-phase voltage source converters under unbalanced grid conditions," *IEEE Trans. Power Electron.*, vol. 34, no. 11, pp. 11278–11289, Nov. 2019.

[16] S. D'Arco, J. A. Suul, and O. B. Fosso, "Automatic tuning of cascaded controllers for power converters using eigenvalue parametric sensitivities," *IEEE Trans. Ind. Appl.*, vol. 51, no. 2, pp. 1743–1753, Mar. 2015.

[17] M. Hamzeh, S. Emamian, H. Karimi, and J. Mahseredjian, "Robust control of an islanded microgrid under unbalanced and nonlinear load conditions," *IEEE Trans. Emerg. Sel. Topics Power Electron.*, vol. 4, no. 2, pp. 512–520, Jun. 2016.

[18] M. Raeispour, H. Atrianfar, H. R. Baghaee, and G. B. Gharehpetian, "Robust hierarchical control of VSC-based off-grid AC microgrids to enhancing stability and FRT capability considering time-varying delays," *IEEE J. Emerg. Sel. Topics Power Electron.*, vol. 9, no. 6, pp. 7159–7172, Dec. 2021.

[19] S. Derakhshan, M. Shafiee-Rad, Q. Shafiee, and M. R. Jahed-Motlagh, "Decentralized robust LMI-based voltage control strategy for autonomous inverter-interfaced multi-DG microgrids," *IEEE Trans. Power Syst.*, early access, Sep. 6, 2022, doi: 10.1109/TPWRS.2022.3204625.

[20] M. Shafiee-Rad, Q. Shafiee, M. S. Sadabadi, and M. R. Jahed-Motlagh, "Decentralized voltage stabilization and robust performance satisfaction of islanded inverter-interfaced microgrids," *IEEE Syst. J.*, vol. 15, no. 2, pp. 1893–1904, Jun. 2021.

[21] H. R. Baghaee, M. Mirsalim, G. B. Gharehpetian, and H. A. Talebi, "Decentralized sliding mode control of WG/PV/FC microgrids under unbalanced and nonlinear load conditions for on-and off-grid modes," *IEEE Syst. J.*, vol. 12, no. 4, pp. 3108–3119, Dec. 2018.

[22] M. Babazadeh and A. Nobakhti, "Robust decomposition and structured control of an islanded multi-DG microgrid," *IEEE Trans. Smart Grid*, vol. 10, no. 3, pp. 2463–2474, May 2019.

[23] M. S. Sadabadi, Q. Shafiee, and A. Karimi, "Plug-and-play voltage stabilization in inverter-interfaced microgrids via a robust control strategy," *IEEE Trans. Control Syst. Technol.*, vol. 25, no. 3, pp. 781–791, May 2017.

[24] T. Dragičević, "Model predictive control of power converters for robust and fast operation of AC microgrids," *IEEE Trans. Power Electron.*, vol. 33, no. 7, pp. 6304–6317, Jul. 2018.

[25] M. Cucuzzella, G. P. Incremona, and A. Ferrara, "Decentralized sliding mode control of islanded AC microgrids with arbitrary topology," *IEEE Trans. Ind. Electron.*, vol. 64, no. 8, pp. 6706–6713, Aug. 2017.

[26] M. B. Delghavi and A. Yazdani, "Sliding-mode control of AC voltages and currents of dispatchable distributed energy resources in master-slave-organized inverter-based microgrids," *IEEE Trans. Smart Grid*, vol. 10, no. 1, pp. 980–991, Jan. 2019.

[27] J. R. Massing, M. Stefanello, H. A. Grundling, and H. Pinheiro, "Adaptive current control for grid-connected converters with LCL filter," *IEEE Trans. Ind. Electron.*, vol. 59, no. 12, pp. 4681–4693, Dec. 2012.

[28] J.-W. Jung, N. T.-T. Vu, D. Q. Dang, T. D. Do, Y.-S. Choi, and H. H. Choi, "A three-phase inverter for a standalone distributed generation system: Adaptive voltage control design and stability analysis," *IEEE Trans. Energy Convers.*, vol. 29, no. 1, pp. 46–56, Mar. 2014.

[29] M. Rubagotti, A. Estrada, F. Castanos, A. Ferrara, and L. Fridman, "Integral sliding mode control for nonlinear systems with matched and unmatched perturbations," *IEEE Trans. Autom. Control*, vol. 56, no. 11, pp. 2699–2704, Nov. 2011.

[30] G. Song and G. Tao, "A partial-state feedback model reference adaptive control scheme," *IEEE Trans. Autom. Control*, vol. 65, no. 1, pp. 44–57, Jan. 2020.

[31] L. Wen, G. Tao, and Y. Liu, "Multivariable adaptive output rejection of unmatched input disturbances," *Int. J. Adapt. Control Signal Process.*, vol. 30, nos. 8–10, pp. 1203–1227, Aug. 2016.

[32] S. Sahoo, S. Mishra, S. Jha, and B. Singh, "A cooperative adaptive droop based energy management and optimal voltage regulation scheme for DC microgrids," *IEEE Trans. Ind. Electron.*, vol. 67, no. 4, pp. 2894–2904, Apr. 2020.

[33] A. Afshari, M. Karrari, H. R. Baghaee, G. B. Gharehpetian, and J. M. Guerrero, "Robust cooperative control of isolated AC microgrids subject to unreliable communications: A low-gain feedback approach," *IEEE Syst. J.*, vol. 16, no. 1, pp. 55–66, Mar. 2022.

[34] N. M. Dehkordi and S. Z. Moussavi, "Distributed resilient adaptive control of islanded microgrids under Sensor/Actuator faults," *IEEE Trans. Smart Grid*, vol. 11, no. 3, pp. 2699–2708, May 2020.

[35] A. Afshari, M. Karrari, H. R. Baghaee, and G. B. Gharehpetian, "Resilient synchronization of voltage/frequency in AC microgrids under deception attacks," *IEEE Syst. J.*, vol. 15, no. 2, pp. 2125–2136, Jun. 2021.

[36] G. Tao, "Multivariable adaptive control: A survey," *Automatica*, vol. 50, no. 11, pp. 2737–2764, 2014.

[37] A. Tayyebi, A. Anta, and F. Dorfler, "Grid-forming hybrid angle control and almost global stability of the DC–AC power converter," *IEEE Trans. Autom. Control*, early access, Jul. 26, 2022, doi: 10.1109/TAC.2022.3193953.

[38] M. Davari, A. Aghazadeh, W. Gao, and F. Blaabjerg, "Detailed dynamic DC models of VSC considering controls for DC-fault simulations in modernized microgrid protection," *IEEE J. Emerg. Sel. Topics Power Electron.*, vol. 9, no. 4, pp. 4514–4532, Aug. 2021.

[39] I. Subotic and D. Gros, "Power-balancing dual-port grid-forming power converter control for renewable integration and hybrid AC/DC power systems," *IEEE Trans. Control Netw. Syst.*, vol. 9, no. 4, pp. 1949–1961, Dec. 2022.

[40] F. Degioanni, I. G. Zurbriggen, and M. Ordonez, "Enhanced DC-link voltage dynamics for grid-connected converters," *IEEE Trans. Ind. Electron.*, vol. 69, no. 11, pp. 10787–10796, Nov. 2022.

[41] Y. Gui, F. Blaabjerg, X. Wang, J. D. Bendtsen, D. Yang, and J. Stoustrup, "Improved DC-link voltage regulation strategy for grid-connected converters," *IEEE Trans. Ind. Electron.*, vol. 68, no. 6, pp. 4977–4987, Jun. 2021.

[42] M. Davari and Y. A.-R. I. Mohamed, "Dynamics and robust control of a grid-connected VSC in multiterminal DC grids considering the instantaneous power of DC- and AC-side filters and DC grid uncertainty," *IEEE Trans. Power Electron.*, vol. 31, no. 3, pp. 1942–1958, Mar. 2016.

[43] G. Tao, *Adaptive Control Design and Analysis*, 1st ed. Hoboken, NJ, USA: Wiley, Jul. 2003, doi: 10.1002/0471459100.

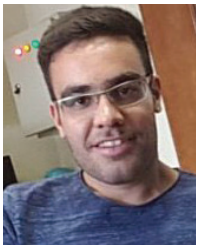

Amir Afshari received the B.Sc. degree in electrical engineering from the Qom University of Technology, Qom, Iran, in 2016, and the M.Sc. degree in electrical engineering from the Amirkabir University of Technology, Tehran, Iran, in 2020. He is currently pursuing the Ph.D. degree in electrical and computer engineering with the University of Wisconsin–Madison, USA. His research interests include controls of modern power grids with high-penetration of power-electronics-based systems.

Masoud Davari (Senior Member, IEEE) was born in Isfahan, Iran, in September 1985. He received the B.Sc. degree (summa cum laude) in electrical engineering (power) from the Isfahan University of Technology, Isfahan, in 2007, the M.Sc. degree (summa cum laude) in electrical engineering (power) from the Amirkabir University of Technology (Tehran Polytechnic), Tehran, Iran, in 2010, and the Ph.D. degree (Hons.) in electrical engineering (power electronics in energy systems) from the University of Alberta, Edmonton, AB, Canada, in 2016.

He was with the Grid Secure Operation Research Center, Iran, and the Electric Power Research Institute (EPRI), Tehran, from January 2010 to December 2011. From April 2015 to June 2017, he was a Senior Research and Development Specialist and a Senior Consultant with Quanta-Technology Company, Markham, ON, Canada, in the field of the dynamic interaction of renewables with smart ac/dc grids and control, protection, and the automation of microgrids. In July 2017, he joined as a tenure-track Assistant Professor with the Allen E. Paulson College of Engineering and Computing, Department of Electrical and Computer Engineering, Georgia Southern University (GSU), Statesboro, GA, USA, where he was recommended for being granted "early" promotion to an Associate Professor and the Award of "early" Tenure in December 2021, and officially approved for both in February 2022. He is currently the Founder and the Director of the Laboratory for Advanced Power and Energy Systems [LAPES (watch it on https://www.youtube.com/watch?v=mhVHp7uMNKo)], State-of-the-Art Center for Engineering and Research (CEaR), GSU, in 2021. He has developed and implemented several experimental test rigs for research universities and the power and energy industry. He has authored several papers published in IEEE TRANSACTIONS and journals. His research interests include the dynamics, controls, the protections of different power electronic converters utilized in the hybrid ac/dc smart grids, and hardware-in-the-loop (HIL) simulation-based testing of modernized power systems.

Dr. Davari has been an active member and the Chapter Lead with the IEEE Power and Energy Society Task Force on "Innovative Teaching Methods for Modern Power and Energy Systems" since July 2020. He has been an active member and the Chapter Lead (for Chapter 3) with the IEEE Working Group P2004—a newly established IEEE working group titled "Hardware-in-the-Loop (HIL) Simulation Based Testing of Electric Power Apparatus and Controls" for IEEE Standards Association since June 2017. He is an invited member of the Golden Key International Honour Society. He was a recipient of the 2019–2020 Allen E. Paulson College of Engineering and Computing (CEC) Faculty Award for Outstanding Scholarly Activity in the Allen E. Paulson CEC at GSU, the Discovery and Innovation Award from the 2020–2021 University Awards of Excellence at GSU, and one of the awardees of the 2021–2022 Impact Area Accelerator Grants (partially funded) at GSU. He was the Chair of the Literature Review Subgroup of DC@Home Standards for the IEEE Standards Association from April 2014 to October 2015. He is an invited Reviewer of several IEEE TRANSACTIONS/JOURNALS, IET journals, *Energies* journal, and various IEEE conferences, the invited speaker at different universities and in diverse societies, and the best Reviewer of the IEEE TRANSACTIONS ON POWER SYSTEMS in 2018 and 2020.

Mehdi Karrari (Senior Member, IEEE) received the Ph.D. degree in control engineering from Sheffield University, Sheffield, U.K., in 1991. Since 1991, he has been with the Amirkabir University of Technology, Tehran, Iran. He has authored or coauthored more than 150 technical articles and three books. His main research interests include power system modeling, modeling and identification of nonlinear dynamic systems, and large-scale and distributed systems.

Weinan Gao (Senior Member, IEEE) received the B.Sc. degree in automation and the M.Sc. degree in control theory and control engineering from Northeastern University, Shenyang, China, in 2011 and 2013, respectively, and the Ph.D. degree in electrical engineering from New York University, Brooklyn, NY, USA in 2017.

He is currently a Professor with the State Key Laboratory of Synthetical Automation for Process Industries, Northeastern University. Previously, he was an Assistant Professor of Mechanical and Civil Engineering with the Florida Institute of Technology, Melbourne, FL, USA; an Assistant Professor of Electrical and Computer Engineering with Georgia Southern University, Statesboro, GA, USA; and a Visiting Professor with the Mitsubishi Electric Research Laboratory (MERL), Cambridge, MA, USA. His research interests include reinforcement learning, adaptive dynamic programming (ADP), optimal control, cooperative adaptive cruise control (CACC), intelligent transportation systems, sampled-data control systems, and output regulation theory. He was a recipient of the Best Paper Award in IEEE International Conference on Real-time Computing and Robotics (RCAR) in 2018 and the David Goodman Research Award at New York University in 2019. He is an Associate Editor of IEEE TRANSACTIONS ON NEURAL NETWORKS AND LEARNING SYSTEMS, IEEE/CAA JOURNAL OF AUTOMATICA SINICA, *Control Engineering Practice*, *Neurocomputing*, and IEEE TRANSACTIONS ON CIRCUITS AND SYSTEMS—II: EXPRESS BRIEFS. He is an Editorial Board Member of *Neural Computing and Applications* and a Technical Committee Member of IEEE Control Systems Society on Nonlinear Systems and Control and IFAC TC 1.2 Adaptive and Learning Systems.

Frede Blaabjerg (Fellow, IEEE) received the Ph.D. degree in electrical engineering from Aalborg University, Aalborg, Denmark, in 1995.

From 1987 to 1988, he was with ABBScandia, Randers, Denmark. He became an Assistant Professor, an Associate Professor, and a Full Professor of Power Electronics and Drives with Aalborg University, in 1992, 1996, and 1998, respectively. In 2017, he became a Villum Investigator. He is also a Honoris Causa with University Politehnica Timisoara (UPT), Timisoara, Romania, and Tallinn Technical University, Tallin, Estonia. He has authored or coauthored four monographs, published more than 600 journal articles in the fields of power electronics and its applications, and was an editor of ten books in power electronics and its applications. His current research interests include power electronics and its applications, such as in wind turbines, PV systems, reliability, harmonics, and adjustable speed drives. He was a recipient of the 33 IEEE Prize Paper Awards, the IEEE PELS Distinguished Service Award in 2009, the EPE-PEMC Council Award in 2010, the IEEE William E. Newell Power Electronics Award 2014, the Villum Kann Rasmussen Research Award 2014, the Global Energy Prize in 2019, and the 2020 IEEE Edison Medal. From 2006 to 2012, he was the Editor-in-Chief for the IEEE TRANSACTIONS ON POWER ELECTRONICS. From 2005 to 2007, he was a Distinguished Lecturer of the IEEE Power Electronics Society and the IEEE Industry Applications Society from 2010 to 2011 and from 2017 to 2018. From 2019 to 2020, he was the President of IEEE Power Electronics Society. He was the Vice President of the Danish Academy of Technical Sciences, Lyngby, Denmark. From 2014 to 2020, he was nominated by Thomson Reuters, Toronto, Canada, to be between the most 250 cited researchers in engineering in the world.